SCIENCE CHINA Materials ARTICLES

mater.scichina.com link.springer.com

Published online 31 January 2018 | https://doi.org/10.1007/s40843-017-9205-x
Sci China Mater 2018, 61(4): 619–628

SPECIAL ISSUE: Advances in Metallic Biomaterials

In vitro and *in vivo* studies on as-extruded Mg-5.25wt.%Zn-0.6wt.%Ca alloy as biodegradable metal

Xuenan Gu[1,2*], Fan Wang[1], Xinhui Xie[3], Mingyi Zheng[4], Ping Li[1,2], Yufeng Zheng[5], Ling Qin[3] and Yubo Fan[1,2,6*]

ABSTRACT **Magnesium alloys have shown prospective applications as a new biodegradable metal within bone. To garantee the longterm biocompatibility, a Mg-Zn-Ca alloy, composing of essential elements for human, was prepared and its feasibility for orthopedic applications was investigated. The *in vitro* and *in vivo* corrosion of Mg-Zn-Ca alloy as well as the biocompatibility were studied. The *in vitro* corrosion tests in five kinds of physiological solutions showed that the corrosion rates and corrosion morphologies of the alloy were strongly influenced by the solution used. The addition of serum in Hank's and MEM significantly slowed down the corrosion rate and improved the corrosion uniformity of the alloy. The corrosion rate decreased with increasing serum concentration. The alloy showed the slowest corrosion rate as well as homogeneous corrosion morphology in MEM+10%FBS. Both the indirect and direct cell experiments indicated good cytocompatibility of the extruded Mg-Zn-Ca alloy. *In vivo*, we observed a gradual degradation process from the surface of extruded Mg-Zn-Ca alloy and only 40% in volume of implant was left after 4 weeks implantation in medullary cavities of mice. The micro-CT and histological analyses revealed its good biocompatibility with peri-implant new bone formation and increasing cortical bone thickness with increasing implantation period. This study showed that the extruded Mg-Zn-Ca alloy provided sufficient biocompatibility for orthopedic application, though the *in vivo* corrosion rate should be further reduced for clinical use.**

Keywords: magnesium alloy, corrosion, biocompatibility, bone, biomaterial

INTRODUCTION

Metallic biomaterials have been widely used as orthopedic implants. Traditionally, there is a focus on improving the corrosion resistance of metallic biomaterials, not only because corrosion determines the service life of devices, but also due to the side effects caused by the corrosion products [1–3]. In some clinical applications, such as fracture treatment, permanent metal implants are not necessary or even disadvantageous [4]. Degradable biomaterials would be much more suitable for temporary implants, which could assist in bone healing and gradually dissolve without implant residues, and hence a second surgery for implant removal can be avoided.

Magnesium alloys are promising candidates for temporary implants [5–9]. Magnesium alloys can corrode gradually in physiological environment. The releasing of magnesium is not harmful but beneficial to new bone growth around the magnesium implants. Excessive magnesium will be excreted in the urine. For orthopedics, magnesium alloys have high specific strength and its elastic modulus is close to bone which helps to eliminate the stress shielding effect. For orthopedic use, a slow homogeneous corrosion, adequate mechanical strength as well as the sufficient biocompatibility was recommended for magnesium alloys.

A number of magnesium alloys have been under investigation. Aluminum (Al) and rare earth elements (REEs) were usually used to elevate the strength of magnesium and to reduce the corrosion rate. Some Al- and REEs-containing alloys, such as AZ91 [10], LAE442

[1] School of Biological Science and Medical Engineering, Beihang University, Beijing 100083, China
[2] Beijing Advanced Innovation Centre for Biomedical Engineering, Beihang University, Beijing 102402, China
[3] Department of Orthopaedics and Traumatology, The Chinese University of Hong Kong, Hong Kong, China
[4] School of Materials science and Engineering, Harbin Institute of Technology, Harbin 150001, China
[5] Department of Materials Science and Engineering, College of Engineering, Peking University, Beijing 100871, China
[6] National Research Center for Rehabilitation Technical Aids, Beijing 100176, China
* Corresponding authors (emails: xngu@buaa.edu.cn (Gu X); yubofan@buaa.edu.cn (Fan Y))

[10,11], WZ21 [12] and Mg-Nd-Zn-Zr [13], were tested. Al is a well-known neurotoxicant and associated with dementia and Alzheimer's disease [14]. Highly concentrated REEs were observed in different inner organs in rabbits after long-term implantation of rare earth-containing magnesium alloys [11]. Hence, the inclusion of Al and REE in magnesium alloys is controversial from a medical point of view. The elements that exist in the human body and also retard the corrosion of magnesium alloys are promising candidates for alloying. Calcium is one of the major components in human bone and the release of Ca ions may improve the bone healing process. Our previous study on binary Mg-Ca alloys reported the dose-dependent effect of Ca on the materials' mechanical and corrosion properties [15,16]. The corrosion of Mg-Ca alloy was reduced by the addition of Ca up to 1 wt.%, while higher Ca addition resulted in increased corrosion rate [15]. Zinc is an essential trace element in human body and has basic safety for biomedical use. Additionally, zinc contributes to the overall strength of magnesium alloys due to the solid solution and precipitation strengthening effect [17]. Yan *et al.* [18] demonstrated that Mg-Zn alloy performed better than Ti-3Al-2.5V by promoting healing and reducing inflammation. Based on the aforementioned considerations, several Mg alloys have been investigated with the addition of different contents of Ca and Zn [19–22]. All the previous studies acknowledge the biosafety of Ca and Zn addition in magnesium and support the great potential of Ca- and Zn-containing magnesium alloys for implant applications.

Our previous study has demonstrated that Mg-5.25Zn-0.6Ca alloy may offer a good combination of high strength and simultaneously high ductility. The yield strength ranged in 130–250 MPa, tensile strength ranged in 220–330 MPa and the elongation ranged in 12%–27% [23,24]. The mechanical properties meet the requirements of magnesium alloys for bone use [13]. The purpose of this study is to investigate the *in vitro* and *in vivo* corrosion as well as the biocompatibility of Mg-5.25Zn-0.6Ca alloy to take further insight into the feasibility for orthopedic application.

EXPERIMENTAL SECTION

Materials preparation

The material used in this investigation was an extruded Mg-Zn-Ca alloy having a composition of Mg-5.25wt.%Zn -0.6wt.%Ca. The cast ingot was indirect-extruded with an extrusion ratio of 20:1 at 300°C. The specific processing route and microstructures of extruded Mg-Zn-Ca were described in our previous work [15,23]. Disk samples, with 12.0 mm in diameter and 2.0 mm in thickness, were cut from the extruded bars for the *in vitro* corrosion and cell culture experiments. Cylindrical rods with 0.7 mm in diameter and 5.0 mm in length were machined from the extruded bars as intramedullary nail for implantation in mice. Each sample was mechanically polished with SiC paper up to 2000 grit and ultrasonically cleaned in acetone, absolute ethanol and distilled water for 10 min each. All samples were sterilized by ethylene oxide (ETO) before testing.

Corrosion test

The corrosion behavior of magnesium alloys is very sensitive to the aggressive environment. It was reported that the corrosion rates varied by a factor of 100, depending on the different compositions of solutions, i.e., buffer, protein [25]. Therefore, five test solutions including Hank's solution, minimum essential medium (MEM) and those solutions supplemented with different concentrations of fetal bovine serum (FBS) were used. The ion concentrations in the five solutions are presented in Table 1.

The hydrogen evolution tests were carried out in the five solutions following the protocol described in our previous studies [26–28]. 0.2% Sodium azide was added in the medium to kill the bacterial and the solutions were changed every 2 days. The temperature was kept at 37 ±0.5°C in the water bath. After 7 days immersion, the samples were removed from the solution, rinsed with distilled water and dried in warm air. The corrosion products were removed in chromic acid for 20 min. In addition, changes in the surface morphologies and compositions of the samples after corrosion were observed by an environmental scanning electron microscope (ESEM, Quanta 200FEG) equipped with an energy dispersive spectrometer (EDS). An average of three measurements was taken for each group.

Cytotoxicity tests

Human osteosarcoma cells (MG63) were used in the *in vitro* cell culture experiments. They were cultured in MEM, 10%FBS, 100 U mL^{-1} penicillin and 100 μg mL^{-1} streptomycin in a humidified atmosphere with 5% CO_2 at 37°C. The cytotoxicity of the material was evaluated by both the indirect and direct cell assays.

For the indirect cell assay, extracts were prepared with a surface area to extraction medium ratio of 1 mL cm^{-2} in a humidified atmosphere with 5% CO_2 at 37°C for 72 h

Table 1 Ion concentrations in five corrosion solutions (mmol L^{-1})

	Hank's solution	Hank's +10% FBS	Hank's +20% FBS	MEM	MEM+10% FBS
Na^+	142	142	142	143.3	143.3
K^+	5.9	5.9	5.9	5.4	5.4
Ca^{2+}	1.3	1.3	1.3	1.8	1.8
Mg^{2+}	0.8	0.8	0.8	0.8	0.8
HCO_3^-	4.2	4.2	4.2	26.2	26.2
Cl^-	145	145	145	125.2	125.2
HPO_4^{2-}	0.8	0.8	0.8	0.96	0.96
SO_4^{2-}	0.8	0.8	0.8	0.8	0.8
Glucose	5.6	5.6	5.6	5.6	5.6
Amino acid (g L^{-1})	–	–	–	0.55	0.55
FBS	–	10%	20%	–	10%

incubation. The supernatant fluid was withdrawn, centrifuged and then diluted into 50% and 10% concentrations. MG63 cells were incubated in 96-well cell culture plates at 3×10^4 cells/mL in each well for 24 h to allow attachment. The medium was then replaced with 100 μL extracts. 100 μL MEM+10%FBS medium was used as a negative control and 100 μL 10% dimethyl sulfoxide (DMSO) medium was used as a positive control. After 1, 3 and 5 days culture periods, 10 μL 3-(4,5-dimethyl-2-thiazolyl)-2,5-diphenyl-2H-tetrazolium bromide (MTT) was added to each well followed by incubation for 4 h, and then 100 μL formazan solubilizing solution (10%SDS in 0.01 mol L^{-1} HCl) was added to each well. After further incubation overnight, the spectrophotometric absorbance of each well was measured by a microplate reader (Bio-RAD680) at 570 nm with a reference wavelength of 630 nm.

For the direct cell adhesion assay, 1 mL cell suspensions were seeded onto the samples at a cell density of 5×10^4 cells/mL. After 1 and 3 days culture, the samples were rinsed with PBS for three times and then fixed in 2.5% glutaraldehyde solution for 2 h at room temperature. The samples were then dehydrated in a gradient ethanol/distilled water mixture (50%, 60%, 70%, 80%, 90% and 100%) for 10 min each. The morphologies of the cells adhered to the surfaces of samples were observed by ESEM.

Surgery

Animal experimental protocol was approved by the Animal Ethics Committee of the Chinese University of Hong Kong (Ref. No.10/049/MIS). Eight 3-month old C57BL/6 mice were randomly assigned into two groups (n=4). Animals were generally anesthetized with ketamine (75 mg kg^{-1}) and xylazine (10 mg kg^{-1}) for surgery and the left knee of mice was scrubbed with 25 g L^{-1} tincture of iodine and 70% ethanol. The Mg-Zn-Ca alloy rods were implanted into predrilling holes (0.7 mm in diameter and 5 mm in length) in the left femur along the axial of shaft from distal femur. The predrilled bone tunnel was left empty as the control group. The wounds were then carefully sutured and the mice were housed in an environmentally controlled animal care laboratory after surgery. The change of serum magnesium, zinc and calcium was measured 4 weeks post-surgery, in comparison with the control group.

Radiographic and micro-CT evaluation

The sequential radiographs of the distal femur were taken (30 kV, 3 s) for general inspection of healing process every week post-operation. An *in vivo* micro-computerized tomography (micro-CT, Viva CT40, Scanco Medical AG, Brüttisellen, Switzerland) with a voxel size of 20 μm was used to monitor the degradation of magnesium implants and bone healing in the distal femur of mice every week over 4 weeks post-operation. The two-dimensional (2D) images were acquired directly from the scanning and the three-dimensional (3D) structure was reconstructed by the volume of interest (VOI) where an optimized threshold was used to isolate the bone and implants from the background. The volume changes of implants were measured on the digitally extracted tissue to calculate the *in vivo* corrosion rate [27]. The bone mineral density (BMD) and the cortical bone thickness were also determined.

Histological evaluation

Four weeks post-operation, the explanted femurs were

harvested and fixed in 4% buffered formaldehyde. Followed by gradient dehydration, embedding and polymerization in methylmethacrylate resin, 5 μm thin slices were prepared with a LEICA 2500E microtome. Then the slices were stained with Goldner's trichrome stains, and microscopically examined.

Statistical analysis

Statistical analysis was conducted with SPSS 10.0. Differences between groups were analyzed using an analysis of variance (ANOVA). Statistical significance was defined as $p<0.05$.

RESULTS AND DISCUSSION

In vitro corrosion of Mg-Zn-Ca alloy

Five simulated body fluids were used to evaluate the *in vitro* corrosion of Mg-Zn-Ca alloy. The resulting corrosion behaviors vary significantly depending on the used solution, as shown in Figs 1 and 2. Mg-Zn-Ca alloy exhibits fast corrosion in Hank's solution, with a rough corrosion product layer and broad distribution of corrosion pits beneath the corrosion product layer (Fig. 2a) after 7 d corrosion. Compared to the Hank's solution, a lower corrosion rate is observed for the samples immersed in MEM (Fig. 1). In contrast to the strong localized corrosion attack observed for samples in Hank's solution, the samples in MEM show a more uniform corrosion attack and less distribution of corrosion pits (Fig. 2d). This phenomenon might be related to the increased concentration of bicarbonate from 4.2 mmol L^{-1} (for Hank's solution) to 26.2 mmol L^{-1} (for MEM). Bicarbonate ions reduced the pH value of the solution and thus accelerated the corrosion of AZ31 when [HCO_3^-] <12 mmol L^{-1} [29]. For [HCO_3^-]>12 mmol L^{-1}, $MgCO_3$ was fast precipitated on magnesium surface and suppressed the pitting corrosion [30]. Wagener and Virtanen [31] found high amount of carbonate groups on the surface of magnesium after immersion in DMEM, which may suggest the formation of $MgCO_3$. In addition, the lower concentration of chloride ions (Table 1) may contribute to the slower corrosion rate in MEM than in Hank's solution, since it is known to be notorious for the corrosion of magnesium. Furthermore, Wagener and Virtanen [31] revealed the formation of a double-layered corrosion product layer on magnesium after immersion in DMEM in air, consisting of an inner porous layer and a compact outer layer. The compact outer layer composing of calcium phosphate compounds reduced corrosion significantly.

The addition of serum into the Hank's solution results

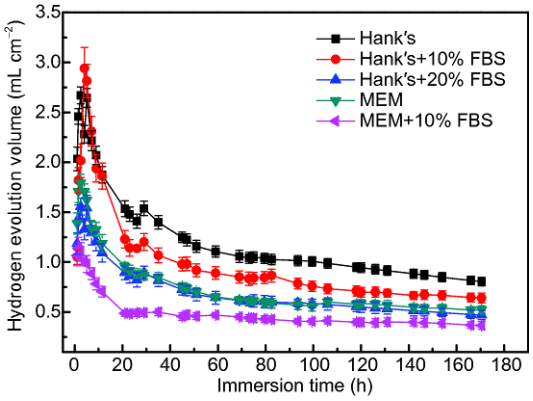

Figure 1 Hydrogen evolution volume of Mg-Zn-Ca alloy as a function of immersion time in different solutions.

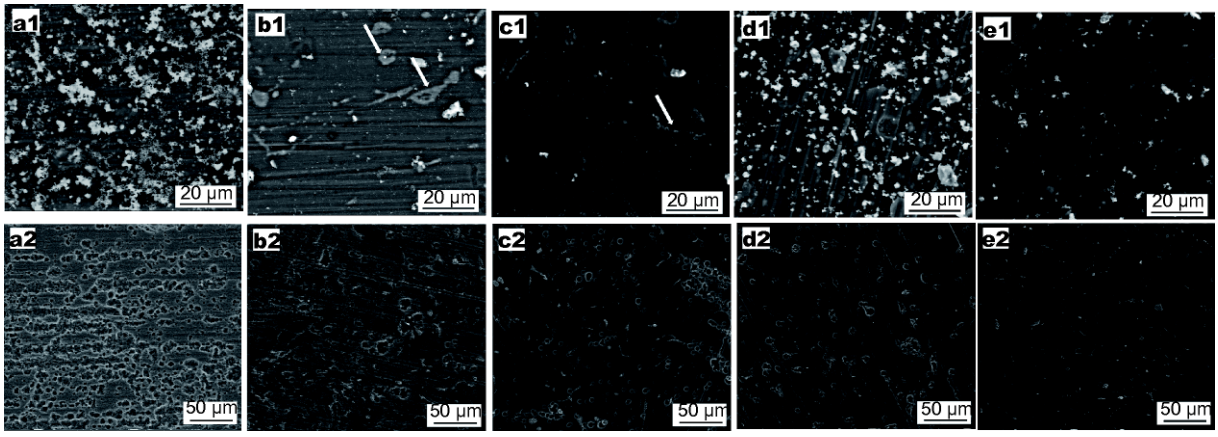

Figure 2 Surface morphologies of the samples immersed in different solutions for 7 days: (a) Hank's solution, (b) Hank's+10%FBS, (c) Hank's+20% FBS, (d) MEM, (e) MEM+10%FBS (1) before and (2) after cleaning the corrosion products by CrO_3. The arrows in (b1) and (c1) indicate the intermetallics in Mg-Zn-Ca alloy.

Table 2 The chemical compositions (wt.%) of the corrosion products of Mg-Zn-Ca alloy after 7 days immersion in different solutions

	C	N	O	Mg	P	S	Ca
Hank's	5.54	–	43.23	17.74	13.06	0.07	20.34
Hank's+10%FBS	7.98	2.08	32.78	39.8	5.64	0.23	11.49
Hank's+20%FBS	16.74	3.17	25.51	43.93	4.48	0.28	5.89
MEM	6.33	1.63	38.95	33.14	7.33	0.13	12.5
MEM+10%FBS	13.2	2.8	25.9	46.7	3.7	0.3	7.3

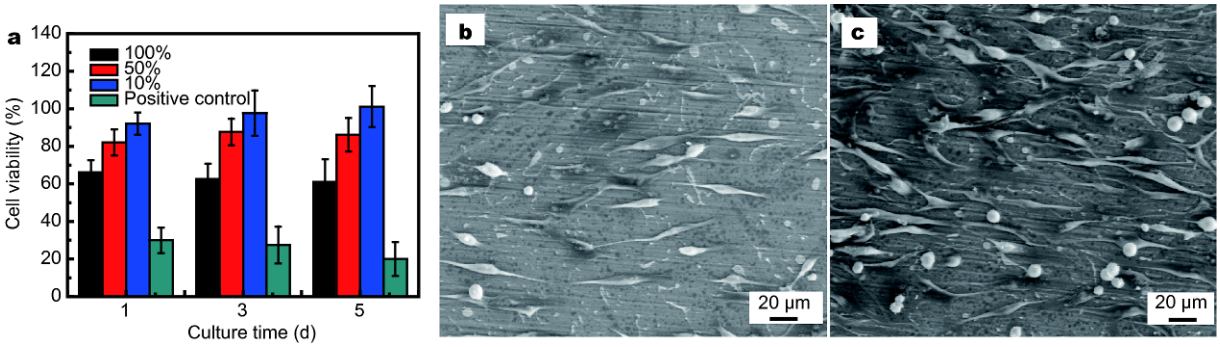

Figure 3 (a) MG63 cell viability of Mg-Zn-Ca alloy extracts diluted with different concentrations; cell morphologies cultured on the samples for (b) 1 and (c) 3 days.

in a significantly reduced corrosion rate of the samples (Fig. 1) as well as a more uniform corrosion surface morphology. Compared to the samples in Hank's solution, a relatively even and thin corrosion product layer is observed on the samples' surface with obvious scratch and intermetallic (arrows in Fig. 2b1, c1). Moreover, less corrosion pits was seen on the samples' surface in Hank's +FBS solution (Fig. 2b2, c2). The EDS results indicate the significant reduction of O, Ca and P weight percentage as well as the increment of Mg intensity on the samples' surface in Hank's+FBS solution (Table 2), demonstrating the less corrosion product precipitation. Moreover, the corrosion rates of the samples decrease with increasing amount of serum concentration (Fig. 1). Serum or proteins certainly influence the magnesium corrosion by chelation reactions with Mg^{2+} and accelerate the dissolution of magnesium [32,33]. On the other hand, proteins would also adhere on magnesium to form a protein-containing protective layer against corrosion [32,34]. Both of these effects depend on the nature of magnesium surface and protein in question. The slower corrosion rates are also observed due to the addition of serum in MEM.

In vitro and *in vivo* biocompatibility of Mg-Zn-Ca alloy

To evaluate the cytocompatibility of Mg-Zn-Ca alloy, both the extract and direct assay were carried out (Fig. 3). Severe cytotoxicity is observed for 100% extract. Similar phenomenon was also reported for 100% magnesium alloy extract, because of the alkaline stress, osmolality [35] or magnesium concentration [36]. After 2 and 10 times dilution, the cytotoxicity is reduced and at Grade 0–1 (see Fig. 3a). In addition, MG63 cells were directly seeded on the Mg-Zn-Ca substrate. Cells attach well on the samples' surfaces with flattened spindle shape after 1 d culture and substantial cell proliferation is observed by day 3, as shown in Fig. 3b, c.

In vivo, all the animals were in a good general condition until sacrifice, indicating no systemic effects of the Mg-Zn-Ca alloy. Fig. 4a shows the radiographs of distal femora with Mg-Zn-Ca implants 0–4 weeks post-surgery. The nature of magnesium degradation is associated with hydrogen gas evolution, which is detectable as the low density shadow in the soft tissue around the implant. The gas shadow is more obvious in the 2D micro-CT tomographs and we observed the gas release right after surgery (Fig. 4d). The gas is generated within bone and spreads from bone to more loose soft tissue, i.e., subcutaneous tissue. Thus the subcutaneous emphysema was observed, which might lead to the displacement of neighboring tissue and the degrading implants [15,27]. A small amount of hydrogen gas release is tolerable because the gap between tissues and implants can be refilled with cells afterwards [20]. However, excessive hydrogen evolution *in vivo* reduced the survival rate of rats with magnesium

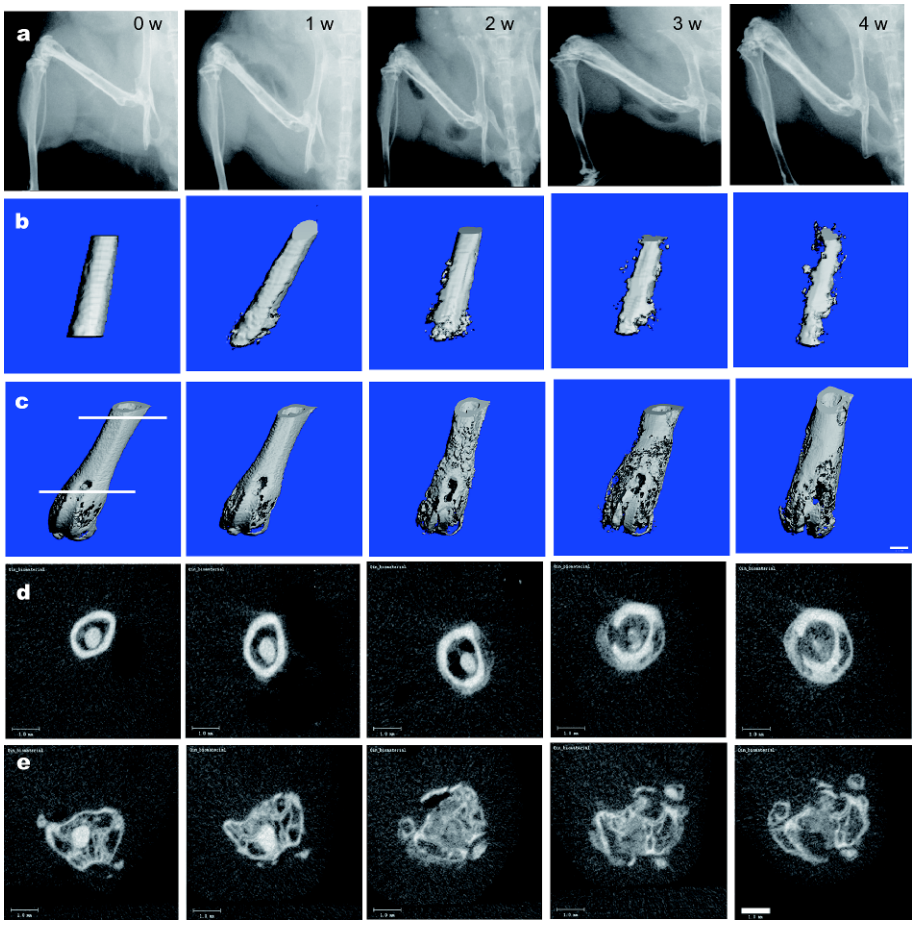

Figure 4 (a) X-ray radiographs of a representative mouse femur with intramedullary implants post-surgery; 3D micro-CT topographies of whole outline of (b) the implant and (c) the distal femur of the mouse; 2D cross-section images from micro-CT at two regions of a representative mouse femur with the implant post-surgery: (d) proximal part of the distal femur and (e) distal part of the distal femur as indicated by the white lines in (c) (scale bar: 1.0 mm).

implants [37]. In the present study, the gas can be quickly exchanged with the surrounding tissue [38] and vanishes without a special treatment. The gas evolution is limited and thus no adverse effect due to the gas formation is detected during the implantation period.

At the same time, peri-implant periosteal reaction is observed since the second week post-surgery (see Fig. 4c). one week post-surgery, the surface of the distal femur was smooth. Some new bone formation was observed in the next two weeks. At week 4, the newly formed bone was integrated and formed a relative smooth surface. From the 2D tomographs of cross-sections of the distal femur, we could see the circumferential osteogenesis with increased cortical bone thickness (Fig. 4d). The peri-implant cortical bone thickness was significantly higher than that of the control 2 weeks post-surgery (p<0.05) and the bone thickness increased with increasing implantation period (Fig. 5a). The micro-CT results show that the thickness of peri-implant cortical bone is ~550±70 μm at week 4. There is no significant difference of peri-implant BMD in the Mg-Zn-Ca alloy and the non-implanted control group during the four weeks implantation period (Fig. 5b).

The histological observation at week 4 post-surgery also shows higher cortical bone thickness (Fig. 5c, d) for the Mg-Zn-Ca alloy group. Additionally, the new bone formation is also observed in the vicinity of implants in the medullary cavity and periosteal area, which is not seen in the control group. An explanation for the new bone formation is the increased concentrations of magnesium in combination with an increase in local pH values, which would enhance the nucleation rate of apatite and improve the mineralization [20,27]. Similarly, a stimulating effect and a significant enhancement in bone formation were

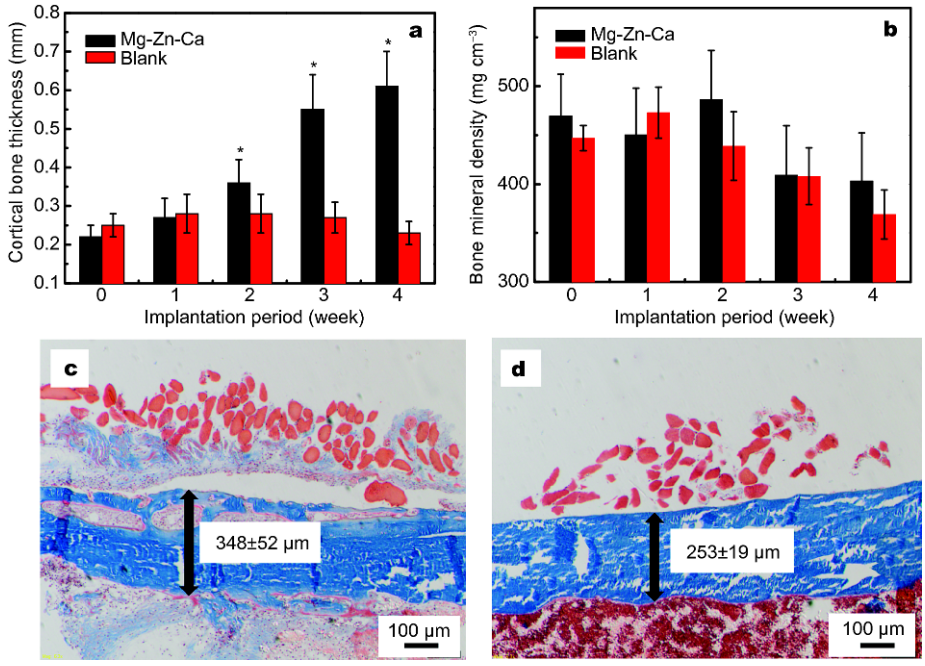

Figure 5 (a) Cortical bone thickness and (b) bone mineral density in the Mg-Zn-Ca alloy and empty control group at different implantation intervals (*p<0.05); representative histology of the cortical bone from (c) the Mg-Zn-Ca alloy and (d) empty control group with Goldner's Trichrome staining at week 4 post-surgery.

also observed around the magnesium implants in previous studies [11,15,20].

In this study, the daily released magnesium is 0.5 mg cm^{-2} day^{-1}, which is far below the daily allowance of magnesium uptake 0.7 g day^{-1} [39]. At week 4 post-surgery, there is no statistically significant difference (p<0.05) of serum magnesium between the magnesium group (20.4±0.4 μg mL^{-1}) and control (21.7±0.7 μg mL^{-1}). The stable serum magnesium level attributes to the homeostatic control of serum magnesium concentrations by kidney and/or bone, which provides a reservoir of large concentrations of magnesium to buffer acute changes in serum magnesium [20]. Moreover, the serum zinc and calcium showed no statistically significant difference (p< 0.05) between the control group (Zn 0.04 ±0.03 μg mL^{-1}, Ca 7.39±0.27 μg mL^{-1}) and the implanted mice 4 weeks post-surgery (Zn 0.03±0.01 μg mL^{-1}, Ca 6.69±0.25 μg mL^{-1}), indicating the good biocompatibility of Mg-Zn-Ca alloy.

In vitro vs. in vivo corrosion of Mg-Zn-Ca alloy

Table 3 compares the *in vitro* and *in vivo* corrosion rates of Mg-Zn-Ca alloys. The *in vivo* corrosion rates start with 1.4 mm y^{-1} 1 week post-surgery but decrease to 0.80 mm y^{-1} 4 weeks post-surgery, indicating that the implants corrode significantly more rapidly *in vivo* than the samples tested in different solutions. The significantly higher *in vivo* corrosion rate is not expected. Generally, the *in vitro* corrosion rates are lower for *in vivo* than *in vitro*. For example, previous studies based on pure magnesium and magnesium alloys (AZ31, Mg-0.8Ca, Mg-1Zn, Mg-1Mn and Mg-1.3Ca-3Zn) showed the *in vivo* corrosion rates tended to be lower than the *in vitro* results tested in EBSS, MEM and MEM with protein [40]. An explanation for the elevated *in vivo* corrosion rate in the present study may involve the trabecular bone and intramedullary implant region selected for implantation. Trabecular bone and medullary cavity are rich in blood supply. Krause *et al.* [41] indicated that the residual WZ21 implants were visible in cortical region, but not in the intramedullary or the soft tissue contact area after 36 weeks implantation. Willbold *et al.* [42] observed that RS66 implants corroded most rapidly in subcutaneous regions followed by intramuscular and intraosseous locations and concluded that the *in vivo* corrosion rates of magnesium alloys are highly dependent on the local blood flow. Moreover, the surgical trauma generated by the drilling process may also contribute to the increased corrosion rate *in vivo*. After the surgical trauma, the oxygen tension and local pH would be reduced and re-

Table 3 The *in vitro* and *in vivo* corrosion rates (mm y^{-1}) of Mg-Zn-Ca alloys

		Corrosion rate (mm y^{-1})			
		1 week	2 weeks	3 weeks	4 weeks
In vivo		1.4±0.15	1.07±0.13	0.85±0.10	0.80±0.09
In vitro	Hank's	0.82±0.04			
	Hank's+10% FBS	0.63±0.05			
	Hank's+20% FBS	0.46±0.04			
	MEM	0.51±0.03			
	MEM+10% FBS	0.35±0.04			

sulted in fast corrosion. Furthermore, Ulmann *et al.* [43] found defects on the surface of intramedullary implantations of LAE442 alloys and the defects led to the faster initial corrosion than the intact implants. In the present study, the implants were tapped in the narrow predrilled bone tunnel, which could have scratched the implant's surface and caused fast initial corrosion [44]. Therefore, we concluded that the implant regions and possibly the surgical procedure resulted in the increased *in vivo* corrosion, compared with the *in vitro* corrosion of Mg-Zn-Ca alloy. Further investigation is needed to explore the reasons for the different *in vitro* and *in vivo* corrosion of magnesium alloys.

CONCLUSIONS

In this study, *in vitro* and *in vivo* corrosion performance and resulting biological response of the Mg-Zn-Ca alloy were studied to evaluate its potential as a biodegradable orthopedic material. The alloy exhibited different corrosion rates as well as corrosion morphologies in five solutions. With the addition of serum, the alloy showed improved pitting resistance and decreased corrosion rate. The corrosion rates of alloy decreased with increasing serum concentration. The slowest corrosion rate and homogeneous corrosion morphology was observed for alloy in MEM containing 10% FBS. The alloy showed no toxic risks to MG63 cells in 50% and 10% concentration of extracts. MG63 cells could adhere, spread and proliferate on the alloy's surface. The animal studies reveal a promising *in vivo* biocompatibility of the Mg-Zn-Ca alloy, with increased new bone formation and an acceptable host response. However, Mg-Zn-Ca alloy exhibits fast corrosion in medullary cavities and the corrosion should be further reduced for clinical use.

Received 12 October 2017; accepted 3 January 2018; published online 31 January 2018

1 Antunes RA, de Oliveira MCL. Corrosion fatigue of biomedical metallic alloys: Mechanisms and mitigation. Acta Biomater, 2012, 8: 937–962
2 Chen Q, Thouas GA. Metallic implant biomaterials. Mater Sci Eng-R-Rep, 2015, 87: 1–57
3 Raducanu D, Vasilescu E, Cojocaru VD, *et al.* Mechanical and corrosion resistance of a new nanostructured Ti–Zr–Ta–Nb alloy. J Mech Behav Biomed Mater, 2011, 4: 1421–1430
4 Zhao X, Niinomi M, Nakai M, *et al.* Development of high Zr-containing Ti-based alloys with low Young's modulus for use in removable implants. Mater Sci Eng-C, 2011, 31: 1436–1444
5 Wang J, Smith CE, Sankar J, *et al.* Absorbable magnesium-based stent: physiological factors to consider for *in vitro* degradation assessments. Regenerat Biomater, 2015, 2: 59–69
6 Zheng YF, Gu XN, Witte F. Biodegradable metals. Mater Sci Eng-R-Rep, 2014, 77: 1–34
7 Zeng RC, Cui L, Jiang K, *et al. In vitro* corrosion and cytocompatibility of a microarc oxidation coating and poly(l-lactic acid) composite coating on Mg–1Li–1Ca alloy for orthopedic implants. ACS Appl Mater Interfaces, 2016, 8: 10014–10028
8 Windhagen H, Radtke K, Weizbauer A, *et al.* Biodegradable magnesium-based screw clinically equivalent to titanium screw in hallux valgus surgery: short term results of the first prospective, randomized, controlled clinical pilot study. Biomed Eng Online, 2013, 12: 62
9 Liu Y, Zheng Y, Hayes B. Degradable, absorbable or resorbable—what is the best grammatical modifier for an implant that is eventually absorbed by the body? Sci China Mater, 2017, 60: 377–391
10 Witte F, Kaese V, Haferkamp H, *et al. In vivo* corrosion of four magnesium alloys and the associated bone response. Biomaterials, 2005, 26: 3557–3563
11 Angrisani N, Reifenrath J, Zimmermann F, *et al.* Biocompatibility and degradation of LAE442-based magnesium alloys after implantation of up to 3.5 years in a rabbit model. Acta Biomater, 2016, 44: 355–365
12 Grünewald TA, Ogier A, Akbarzadeh J, *et al.* Reaction of bone nanostructure to a biodegrading magnesium WZ21 implant—A scanning small-angle X-ray scattering time study. Acta Biomater, 2016, 31: 448–457
13 Ding W. Opportunities and challenges for the biodegradable magnesium alloys as next-generation biomaterials. Regen Biomater, 2016, 3: 79–86
14 Witte F, Hort N, Vogt C, *et al.* Degradable biomaterials based on magnesium corrosion. Curr Opin Solid State Mater Sci, 2008, 12: 63–72
15 Li Z, Gu X, Lou S, *et al.* The development of binary Mg–Ca alloys for use as biodegradable materials within bone. Biomaterials, 2008, 29: 1329–1344

16 Zheng YF, Gu XN, Xi YL, *et al.* *In vitro* degradation and cytotoxicity of Mg/Ca composites produced by powder metallurgy. Acta Biomater, 2010, 6: 1783–1791
17 Cai S, Lei T, Li N, *et al.* Effects of Zn on microstructure, mechanical properties and corrosion behavior of Mg–Zn alloys. Mater Sci Eng-C, 2012, 32: 2570–2577
18 Yan J, Chen Y, Yuan Q, *et al.* Comparison of the effects of Mg–6Zn and Ti–3Al–2.5V alloys on TGF-β/TNF-α/VEGF/b-FGF in the healing of the intestinal tract *in vivo*. Biomed Mater, 2014, 9: 025011
19 Bakhsheshi-Rad HR, Hamzah E, Fereidouni-Lotfabadi A, *et al.* Microstructure and bio-corrosion behavior of Mg-Zn and Mg-Zn-Ca alloys for biomedical applications. Mater Corrosion, 2014, 65: 1178–1187
20 Amerstorfer F, Fischerauer SF, Fischer L, *et al.* Long-term *in vivo* degradation behavior and near-implant distribution of resorbed elements for magnesium alloys WZ21 and ZX50. Acta Biomater, 2016, 42: 440–450
21 Hofstetter J, Martinelli E, Pogatscher S, *et al.* Influence of trace impurities on the *in vitro* and *in vivo* degradation of biodegradable Mg–5Zn–0.3Ca alloys. Acta Biomater, 2015, 23: 347–353
22 Wang H, Guan S, Wang Y, *et al.* *In vivo* degradation behavior of Ca-deficient hydroxyapatite coated Mg–Zn–Ca alloy for bone implant application. Colloids Surfs B-Biointerfaces, 2011, 88: 254–259
23 Tong LB, Zheng MY, Cheng LR, *et al.* Influence of deformation rate on microstructure, texture and mechanical properties of indirect-extruded Mg–Zn–Ca alloy. Mater Characterization, 2015, 104: 66–72
24 Tong LB, Zheng MY, Hu XS, *et al.* Influence of ECAP routes on microstructure and mechanical properties of Mg–Zn–Ca alloy. Mater Sci Eng-A, 2010, 527: 4250–4256
25 Waizy H, Seitz JM, Reifenrath J, *et al.* Biodegradable magnesium implants for orthopedic applications. J Mater Sci, 2013, 48: 39–50
26 Gu XN, Li N, Zhou WR, *et al.* Corrosion resistance and surface biocompatibility of a microarc oxidation coating on a Mg–Ca alloy. Acta Biomater, 2011, 7: 1880–1889
27 Gu XN, Xie XH, Li N, *et al.* *In vitro* and *in vivo* studies on a Mg–Sr binary alloy system developed as a new kind of biodegradable metal. Acta Biomater, 2012, 8: 2360–2374
28 Willbold E, Gu X, Albert D, *et al.* Effect of the addition of low rare earth elements (lanthanum, neodymium, cerium) on the biodegradation and biocompatibility of magnesium. Acta Biomater, 2015, 11: 554–562
29 Zeng RC, Hu Y, Guan SK, *et al.* Corrosion of magnesium alloy AZ31: The influence of bicarbonate, sulphate, hydrogen phosphate and dihydrogen phosphate ions in saline solution. Corrosion Sci, 2014, 86: 171–182
30 Xin Y, Huo K, Tao H, *et al.* Influence of aggressive ions on the degradation behavior of biomedical magnesium alloy in physiological environment. Acta Biomater, 2008, 4: 2008–2015
31 Wagener V, Virtanen S. Protective layer formation on magnesium in cell culture medium. Mater Sci Eng-C, 2016, 63: 341–351
32 Esmaily M, Svensson JE, Fajardo S, *et al.* Fundamentals and advances in magnesium alloy corrosion. Prog Mater Sci, 2017, 89: 92–193
33 Yang L, Hort N, Willumeit R, *et al.* Effects of corrosion environment and proteins on magnesium corrosion. Corrosion Eng Sci Tech, 2012, 47: 335–339
34 Yamamoto A, Hiromoto S. Effect of inorganic salts, amino acids and proteins on the degradation of pure magnesium *in vitro*. Mater Sci Eng-C, 2009, 29: 1559–1568
35 Fischer J, Pröfrock D, Hort N, *et al.* Improved cytotoxicity testing of magnesium materials. Mater Sci Eng-B, 2011, 176: 830–834
36 Wang J, Witte F, Xi T, *et al.* Recommendation for modifying current cytotoxicity testing standards for biodegradable magnesium-based materials. Acta Biomater, 2015, 21: 237–249
37 Noviana D, Paramitha D, Ulum MF, *et al.* The effect of hydrogen gas evolution of magnesium implant on the postimplantation mortality of rats. J Orthopaedic Translation, 2016, 5: 9–15
38 Kuhlmann J, Bartsch I, Willbold E, *et al.* Fast escape of hydrogen from gas cavities around corroding magnesium implants. Acta Biomater, 2013, 9: 8714–8721
39 Gu XN, Zheng YF. A review on magnesium alloys as biodegradable materials. Front Mater Sci China, 2010, 4: 111–115
40 Walker J, Shadanbaz S, Kirkland NT, *et al.* Magnesium alloys: Predicting *in vivo* corrosion with *in vitro* immersion testing. J Biomed Mater Res, 2012, 100B: 1134–1141
41 Kraus T, Fischerauer SF, Hänzi AC, *et al.* Magnesium alloys for temporary implants in osteosynthesis: *In vivo* studies of their degradation and interaction with bone. Acta Biomater, 2012, 8: 1230–1238
42 Willbold E, Kalla K, Bartsch I, *et al.* Biocompatibility of rapidly solidified magnesium alloy RS66 as a temporary biodegradable metal. Acta Biomater, 2013, 9: 8509–8517
43 Ullmann B, Reifenrath J, Seitz JM, *et al.* Influence of the grain size on the *in vivo* degradation behaviour of the magnesium alloy LAE442. Proc Inst Mech Eng H, 2013, 227: 317–326
44 Reifenrath J, Marten AK, Angrisani N, *et al.* *In vitro* and *in vivo* corrosion of the novel magnesium alloy Mg–La–Nd–Zr: influence of the measurement technique and *in vivo* implant location. Biomed Mater, 2015, 10: 045021

Acknowledgements This work was supported by the National Natural Science Foundation of China (51401007, 11472032, 11120101001 and 11421202), a foundation for the author of the National Excellent Doctoral Dissertation of China (201463), Young Elite Scientists Sponsorship Program By CAST (2017QNRC001), and the National Key Research and Development Plan (2016YFC1102203 and 2016YFC1101100).

Author contributions Qin L and Zheng Y conceived and designed the experiments; Gu X, Xie X and Zheng M performed the experiments and analyzed the data. Gu X, Wang F, Zheng Y and Fan Y co-wrote the manuscript. Li P provided technical guidance and participated in the data analysis.

Conflict of interest The authors declare no conflict of interest.

Xuenan Gu received her PhD degree in mechanics (biomechanics and biomedical engineering) from Peking University, in 2011. Her research interests focus on the development of degradable metallic biomaterials and surface modification of biomedical magnesium alloys.

Yubo Fan received his PhD degree in biomechanics from Sichuan University, in 1992. His research interests focus on biomechanics and mechanobiology, medical appliances, biomaterials and tissue engineering.

挤压态Mg-5.25wt.%Zn-0.6wt.%Ca可降解镁合金的体内外研究

顾雪楠[1,2*], 王凡[1], 谢鑫荟[3], 郑明毅[4], 李萍[1,2], 郑玉峰[5], 秦岭[3], 樊瑜波[1,2,6*]

摘要 可降解医用镁合金在骨科领域显示出良好的应用前景. 为了保证镁合金的生物相容性, 本文设计了全营养元素组成的Mg-Zn-Ca合金, 研究了其体内外腐蚀及生物相容性. Mg-Zn-Ca合金在五种模拟体液中的腐蚀测试结果表明在Hank's和MEM中添加血清能够降低合金腐蚀速度, 并提高腐蚀均匀性. 血清浓度越高, 合金腐蚀速率越低. Mg-Zn-Ca合金在MEM+10%FBS溶液中腐蚀速率低, 腐蚀形貌均匀. 直接法和间接法的细胞实验结果均显示Mg-Zn-Ca合金具有良好的细胞相容性. 动物实验结果表明, Mg-Zn-Ca合金在小鼠骨髓腔内逐步降解, 4周后残余40 vol.%. micro-CT和组织学观察显示植入体周围有新骨形成, 且随着植入时间延长, 皮质骨厚度增加. 因此, 挤压态Mg-Zn-Ca合金具有良好的生物相容性, 有望用作骨科植入材料, 但是其体内降解速率还应进一步降低.

